SHEAR STRENGTH OF REINFORCED CONCRETE DAPPED-END BEAMS USING MECHANISM ANALYSIS

Keun-Hyeok Yang[a], Ashraf F. Ashour[b], and Jong-Kook Lee[c]

[a] *Corresponding author, Department of Architectural Engineering, Mokpo National University, Mokpo, Jeonnam, South Kore.; Tel.: +82 (0)61 450 2456; Fax.: +82 (0)61 450 6454; E-mail: yangkh@mokpo.ac.kr.*

[b] *EDT1, School of Engineering, Design and Technology, University of Bradford, Bradford, BD7 1DP, U.K.*

[c] *Department of Architectural Engineering, Kumoh National Institute of Technology, Gumi, Gyeongbuk, South Korea.*

K. H. Yang is an assistant professor at Mokpo National University, Korea. He received his MSc and PhD degrees from Chungang University, Korea. He was a visiting research fellow at the University of Bradford, UK. His research interests include ductility, strengthening and shear of reinforced high-strength concrete structures.

A. F. Ashour is a senior lecturer at the University of Bradford, UK. He obtained his BSc and MSc degrees from Mansoura University, Egypt and his PhD degree from Cambridge University, UK. His research interests include shear, plasticity and optimisation of reinforced concrete and masonry structures.

J. K. Lee is an assistant professor at Kumoh National University, Korea. He received his MSc and PhD degrees from Seoul National University, Korea. His research interests include engineering technology and method on construction industry, and development of construction materials.

ABSTRACT

A mechanism analysis based on upper-bound theorem of concrete plasticity is developed to predict the critical failure plane and corresponding shear capacity of reinforced concrete dapped-end beams. Failure modes observed in physical tests of reinforced concrete dapped-end beams are idealized as an assemblage of two moving blocks separated by failure surface of displacement discontinuity. The developed mechanism analysis rationally represents the effect of different parameters on failure modes; as a result, the predicted shear capacity is in good agreement with test results. On the other hand, empirical equations specified in PCI design method and strut-and-tie model based on ACI 318-05 highly underestimate test results. The shear capacity of dapped-end beams predicted by the mechanism analysis and strut-and-tie model decreases with the increase of shear span-to-full beam depth ratio when failure occurs along diagonal cracks originating at the bottom corner of beam full depth, though the shear span-to- full beam depth ratio is ignored in PCI design method.

Keywords: dapped-end beams, failure modes, shear capacity, mechanism analysis, strut-and-tie model.

INTRODUCTION

Reinforced concrete dapped-end beams have many useful applications as drop-in beams between corbels or beam-to-beam connections. They are classified as discontinuity regions (D-regions) caused by abrupt change in beam depth and consequently, stress flow around the discontinuity is

severely disturbed.[1, 2] Mattock and Chan[3] recommended that the nib of dapped end beams may be designed similar to an inverted corbel. However, the main diagonal concrete strut force is resisted by a compression force in corbel columns and a tensile force in hanger reinforcement of dapped end beams.

Although dapped-end beams provide better lateral stability and reduce the construction height of pre-cast concrete floors[1, 2], few studies[2-7] on such member were conducted in the literature. Lu et al.[2] concluded that the shear capacity of dapped-end beams increased with the decrease of effective shear span-to-depth ratio of nib, and increase of nib longitudinal reinforcement and concrete strength. On the other hand, Mattock and Chan[3] showed that dapped-end beams exhibited different failure modes with the variation of nib shear span-to-depth ratio and amount of reinforcement at different locations.

In the present study, a mechanism analysis based on upper-bound theorem of concrete plasticity is developed to assess the failure plane and corresponding shear capacity of dapped-end beams. The effect of different parameters on the critical failure plane and shear capacity of dapped-end beams is investigated using the developed mechanism analysis, empirical equation specified in PCI design method[8], and strut-and-tie model based on ACI 318-05[9].

PCI DESIGN METHOD

Based on tests carried out by Mattock and Chan[3], PCI design method recommended several potential failure modes, as numbered in Fig. 1, to evaluate the shear capacity V_n of dapped-end

beams with an effective shear span-to-depth ratio a_1 / d_d less than 1.0, where a_1 is the effective shear span of nib measured from the center of support to hanger reinforcement and d_d is the effective depth of nib. The shear capacity V_n of dapped-end beams owing to yielding of nib longitudinal reinforcement (failure plane ①) can be determined from:

$$V_n = \frac{M_n - N(h_d - d_d)}{a_1} \tag{1}$$

where $M_n \left[= \phi_s \left(\frac{d_d}{h} - 0.59\phi_s \right) f_c' b h^2 \right]$ is the nominal moment capacity of nib, b and h are the beam width and full depth, respectively, f_c' is the concrete compressive strength, $\phi_s \left(= \frac{A_s f_{ys}}{b h f_c'} \right)$ is the longitudinal reinforcement index of nib, A_s and f_{ys} are the area and yield strength of longitudinal reinforcement of nib, respectively, N is the horizontal tensile force applied at beam support, and h_d is the overall depth of nib. On the other hand, the shear capacity V_n owing to diagonal tensile failure plane ② is given below:

$$V_n = A_v f_{yv} + A_h f_{yh} + 0.166\sqrt{f_c'}\lambda b d_d \tag{2}$$

where A_v and f_{yv} are the area and yield strength of vertical shear reinforcement of nib, respectively, and A_h and f_{yh} are the area and yield strength of horizontal shear reinforcement of nib, respectively, and λ = 1.0 for normal weight concrete, 0.85 for sand-lightweight concrete and 0.75 for all other lightweight concrete. For the diagonal tensile failure of re-entrant corner (failure plane ③), the shear capacity V_n is only dependent on the tensile capacity of hanger reinforcement, ignoring the shear transfer capacity of concrete, as given in Eq. (3) below:

$$V_n = A_{SH} f_{ySH} \tag{3}$$

where A_{SH} and f_{ySH} are the area and yield strength of hanger reinforcement, respectively. On the other hand, the shear capacity V_n due to potential vertical cracks along the interface between nib and full depth beam (failure plane ④) is estimated from the shear friction hypothesis as below:

$$V_n = \sqrt{6.895\mu\lambda bh_d\left(A_s f_{ys} + A_h f_{yh} - N\right)} \geq \text{min of } 0.3\lambda^2 f_c^{'} bh_d \text{ and } 6.895\lambda^2 bh_d \quad (4)$$

where $\mu(=1.4\lambda)$ is the friction coefficient of concrete.

PCI design method specifies that the capacity of each potential failure plane represented in Fig. 1 and predicted from Eqs. (1) to (4) should be separately calculated, and the smallest value would govern the dapped-end beam capacity. Fig. 2 shows the variation of normalized shear capacity $V_n / bhf_c^{'}$ of dapped-end beams without shear reinforcement ($A_v = A_h = 0$) and horizontal loads (N =0) obtained from Eqs (1) to (4) versus the main longitudinal reinforcement index ϕ_s of nib. Other beam details are presented in Fig. 2. As ϕ_s increases, predictions from Eqs (1) and (4) are becoming very large and consequently not critical. Therefore, the critical failure plane of dapped-end beams having ϕ_s more than around 0.02 can be generally formed along concrete strut of nib (failure plane ②) or diagonal cracks originating at re-entrant corner (failure plane ③). Comparing the governing Eqs. (2) and (3) for the two modes of failure ② and ③, the shear capacity of dapped-end beams is likely to be controlled by failure of nib concrete strut (failure plane ②), when $\phi_{SH}\left(=\dfrac{A_{SH} f_{ySH}}{bhf_c^{'}}\right) > \dfrac{0.166\lambda d_d}{\sqrt{f_c^{'}}h}$, regardless of a_1 / d_d and ϕ_s. Thus, PCI design method does not adequately represent the effect of a_1 / d_d, and ϕ_s, and completely ignores the effect of a / h on shear capacity of dapped end beams.

STRUT-AND-TIE MODEL

ACI 318-05[9] recommends the use of strut-and-tie model (STM) for the design of discontinuity regions in reinforced concrete members to which beam theory does not apply. However, it does not provide specific guidance on suitable strut-and-tie models for different cases. Fig. 3 shows a developed schematic strut-and-tie model for dapped-end beams in accordance with ACI 318-05 (Appendix A). The top load applied to the dapped-end beam is carried by struts representing compression stress fields in concrete and tie action of reinforcing bars. In their softened strut-and-tie model, Lu et al. [2] assumed that failure of dapped-end beams is always formed at the concrete strut of nib as observed in their physical tests of dapped end beams with shear span-to-overall depth ratio a/h less than 2.0. However, failure of dapped-end beams based on STM model shown in Fig. 3 may occur owing to yielding of longitudinal reinforcement of nib or hanger reinforcement near re-entrant corner, or compressive crushing of either concrete strut of nib or full depth beam. The failure of concrete strut of full depth beam is commonly generated in the vicinity of the bottom node due to the tensile strain effect of main longitudinal reinforcement. Static analysis of STM model in Fig. 3 produces forces in different struts and ties. Hence, the shear capacity for different failure modes can be obtained and the smallest value of the following four cases governs the capacity of dapped-end beams.

Failure plane ① (Yielding of nib reinforcement):

$$V_n = \left(A_s f_{ys} - N\right)\tan\theta_1 \qquad \text{(5. a)}$$

Failure plane ② (Concrete crushing of nib strut):

$$V_n = \nu_e f_c' b w_{st} \sin\theta_1 \tag{5. b}$$

Failure plane ③ (Yielding of hanger reinforcement):

$$V_n = \frac{A_{SH} f_{ySH}(\sin\theta_2 \cot\theta_3 + \cos\theta_2) - N\sin\theta_2}{\sin\theta_2 \cot\theta_3 + \cos\theta_2 + \cot\theta_1 \sin\theta_2} \tag{5. c}$$

Failure plane ⑤ (Concrete crushing of bottom strut of full depth beam):

$$V_n = \frac{\nu_e f_c' b w_{sb}(\sin\theta_3 + \tan\theta_2 \cos\theta_3) - N\tan\theta_2}{(1 + \cot\theta_1 \tan\theta_2 + \tan\theta_2 \cot\theta_3)} \tag{5. d}$$

where ν_e is the effectiveness factor of concrete, $w_{st}(= 2c_t \cos\theta_1 + l_p \sin\theta_1)$ and $w_{sb}(= 2c_b \cos\theta_3 + 2(a_1 - a_0)\sin\theta_3)$ are widths of nib concrete strut and bottom strut of full depth beam, respectively, c_t and c_b are cover thicknesses of longitudinal reinforcement in nib and full depth beam, respectively, l_p is the width of supporting plate, a_0 is the nominal shear span, measured from the center of support to the interface between nib and full depth beam, and θ_1, θ_2 and θ_3 are the inclination of different concrete struts as shown in Fig. 3, which can be approximately expressed as $\tan^{-1}[(h_d - 2c_t)/a_1]$, $\tan^{-1}[(h_d - 2c_t)\tan\theta_3/(h - d_d - c_b)]$, and $\tan^{-1}[(h - 2c_b)/(a - a_1)]$, respectively. The intersection angle between concrete struts and ties should not be less than 26.5˚ as recommended by ACI 318-05.

ACI 318-05 allows the use of effectiveness factor ν_e of 0.75 for concrete struts having a minimum amount of shear reinforcement given below, regardless of concrete strength and the amount of transverse tensile strains.

$$\sum \frac{A_{si}}{b_w s_i} \sin\gamma_i \geq 0.003 \tag{6}$$

where A_{si} and s_i are the total area and spacing of the i–th layer of reinforcement crossing concrete strut of nib, respectively, and γ_i is the angle between the i–th layer of reinforcement and

concrete strut of nib. The shear reinforcement is recommended to be placed in two orthogonal directions in each face. The value of v_e drops to 0.6 if the minimum shear reinforcement defined in Eq. (6) above is not provided.

Fig. 4 shows the variation of normalized shear capacity $V_n / bhf_c^{'}$ of dapped-end beams without shear reinforcement ($A_v = A_h = 0$) and horizontally applied loads (N =0) against longitudinal reinforcement index ϕ_s of nib obtained from the STM model shown in Fig. 3 as recommended by ACI 318-05. The shear capacity determined due to yielding of longitudinal reinforcement of nib significantly increased with the increase of ϕ_s, similar to PCI design method but that obtained from other failure modes is independent of ϕ_s. Thus, the shear capacity of dapped-end beams is governed by other modes of failure, depending on different parameters; for the case presented in Fig. 4, the yielding of hanger reinforcement rather than concrete crushing of nib or full depth beam struts guides the failure for $\phi_s > 0.025$. The influence of other parameters on the dapped end beam shear capacity obtained from STM model is presented later in this paper.

MECHANISM ANALYSIS

Failure mechanism of dapped-end beams

Failure modes of dapped-end beams subjected to vertical and horizontal loads are generally observed[2-5] in nib, interface between nib and full depth beam, diagonal cracks occurred at the re-entrant corner, or diagonal cracks initiated at the bottom corner of full depth beam. Thus, each failure mechanism can be idealized as an assemblage of two rigid blocks separated by a yield line representing the failure zone along which in-plane displacement discontinuity occurs[10] as depicted

in Fig. 5. Each rigid block has two transitional and one rotational displacement components. Considering boundary conditions at end supports, rigid block *I* undergoes a relative rotation to rigid block *II* around an instantaneous center (I.C.) having X_{ic} and Y_{ic} co-ordinates, where the global origin is assumed at the end support as shown in Fig. 5[11].

Yield line end terminals are located at fixed positions for each mechanism as presented in Fig. 5. It was proved[10, 11] that the optimum shape of yield line is a hyperbola as the energy dissipated along it is less than that dissipated in a straight yield line. The hyperbolic yield line turns into two straight segments when I.C. of relative rotation lies inside or on a circle, the diameter of which is the straight line joining the inner edge of supporting plate and the intersection of hanger reinforcement with the beam top surface as shown in Fig. 5 (a). As pointed out by Ashour and Morley[11], yielding of longitudinal reinforcement forces I.C. to lie at the kink of the yield line with two straight segments.

Material Modelling

Concrete is assumed to be a rigid perfectly plastic material obeying the modified Coulomb failure criteria[10] with zero tension cut-off. The effective compressive strength f_c^* is obtained from the cylinder compressive strength f_c' as below:

$$f_c^* = \nu_e f_c' \tag{7}$$

where ν_e is the effectiveness factor, introduced to account for limited ductility of concrete and to absorb other shortcomings of applying plasticity theory to concrete. Although, there is no unified approach for evaluating the effectiveness factor of concrete, many investigations[10, 12] clearly

showed that the effectiveness factor depends on concrete strength and geometrical properties of reinforced concrete members. In the present study, the formula of Bræstrup[12] modified to accommodate failure plane inclination β_i, combined with Nielsen's model[9] considering the effect of concrete compressive strength is adopted as below:

$$(\nu_e)_i = \left(0.8 - \frac{f_c^{'}}{200}\right)(1 - 0.2/\tan\beta_i) \tag{8}$$

where subscript i indicates the failure plane number given in Fig. 5. Considering the geometrical condition of each failure plane, β_1 and β_2 have the same value of $\tan^{-1}\left(\frac{h_d}{a_1 - l_p/2}\right)$, and β_3, β_4, and β_5 can be obtained from $\tan^{-1}\left(\frac{h_d}{a - a_0 - l_p/2}\right)$, $\frac{\pi}{2}$, and $\tan^{-1}\left(\frac{h}{a - a_0 - l_p/2}\right)$, respectively. The failure plane angle to the member axis in the sliding failure of a material obeying modified Coulomb failure criteria should be greater than $\left(\frac{\pi}{4} - \frac{\varphi}{2}\right)$, where φ = 37° for concrete[10]. Thus, the inclination of failure planes should be larger than 26.5°, which is the same as the minimum inclination of concrete struts specified in ACI 318-05. Steel reinforcement in both tension and compression is assumed to be a rigid perfectly plastic material with yield strength f_y and its dowel action is ignored.

Work Equation

The upper-bound theorem is based on the energy principle, by equating the total internal energy W_I to external work done W_E. The total internal energy mainly depends on the position of I.C. and amount of internal stresses in both concrete along yield line and reinforcement crossing yield lines.

The energy $(W_c)_l$ dissipated in concrete per unit length of yield line is written in the following general form[10, 13]:

$$(W_c)_l = \frac{f_c^*}{2} b\delta(1-\sin\alpha) \tag{9}$$

where δ is the relative displacement rate of rigid block *I* to rigid block *II* and α is the angle between the relative displacement at midpoint of yield line chord and yield line chord as shown in Fig. 5. The relative displacement rate δ can be expressed as $\omega \cdot r$, where r is the distance between midpoint of yield line chord and I.C. and ω is the rotational displacement of rigid block *I*. For a yield line with two straight segments as shown in Fig. 5 (a), one segment of the yield line is under tensile stresses with pure separation ($\alpha_1 = \frac{\pi}{2}$), and it can not contribute to the internal energy due to the assumption of zero tensile concrete strength[12]. Therefore, the total internal energy $(W_c)_i$ dissipated in concrete along the hyperbolic or two straight yield lines can be written in the following general form[10, 13]:

$$(W_c)_i = \frac{(\nu_e)_i f_c^{'}}{2} b\omega_i F(O')_i \tag{10}$$

$$F(O')_i = r_i(1-\sin\alpha_i)L_i \quad \text{and} \quad i \geq 2 \qquad \text{for} \qquad r_2 > h_d/(2\sin\beta_2) \tag{11a}$$

$$F(O')_1 = {L_1}^2 \quad \text{and} \quad i = 1 \qquad \text{for} \qquad r_2 \leq h_d/(2\sin\beta_2) \tag{11b}$$

ω_i and r_i indicate relative rotational displacement of rigid block *I* to rigid block *II* about $(\text{I.C.})_i$ and distance between midpoint of yield line chord i and $(\text{I.C.})_i$, respectively, as shown in Fig. 5 and α_i is the angle between the relative displacement δ_i at chord midpoint and chord of yield line i. Both r_i and α_i in Eq. (11) depend on the position of $(\text{I.C.})_i$, as a result, the energy dissipated in concrete is a function of horizontal and vertical coordinates $(X_{ic}, Y_{ic})_i$ of $(\text{I.C.})_i$.

The relative displacement of reinforcement δ_s can be also expressed as $\omega \cdot r_s$, where ω is the relative rotational displacement of rigid block *I* to rigid block *II* about $(\text{I.C.})_i$ and r_s is the distance

between the intersection point of reinforcing bar j with yield line i and (I.C.)$_i$. Therefore the energy $(W_s)_i$ dissipated in longitudinal and web reinforcement crossing yield line i is calculated from[13]:

$$(W_s)_i = \sum_{j=1}^{n} (\omega)_i (A_{st})_{ij} (f_y)_{ij} (r_s)_{ij} \cos(\alpha_s)_{ij} \tag{12}$$

where n is the number of reinforcing bars crossing yield line i, $(A_{st})_{ij}$ and $(f_y)_{ij}$ are the area and yield strength of reinforcing bar j crossing yield line i, respectively, $(r_s)_{ij}$ is the distance between the intersection point of reinforcing bar j with yield line i and (I.C.)$_i$ and $(\alpha_s)_{ij}$ is the angle between the relative displacement $(\delta_s)_j$ and reinforcing bar j crossing yield line i as shown in Fig. 6. In case of horizontal and vertical reinforcing bars, $\cos(\alpha_s)_{ij}$ can be calculated from $\left|(Y_{ic})_i - y_{ij}\right| / (r_s)_{ij}$ and $\left|(X_{ic})_i - x_{ij}\right| / (r_s)_{ij}$, respectively, where x_{ij} and y_{ij} are the horizontal and vertical coordinates of intersection point of reinforcing bar j and yield line i, respectively.

The external work $(W_E)_i$ done by the vertical load V_n and horizontal load N on rigid block *I* is:

$$(W_E)_i = V_n \omega_i \left|(X_{ic})_i\right| + N\omega_i \left|(Y_{ic})_i\right| \tag{13}$$

Equating the total internal energy dissipated in concrete and reinforcement to external work done, the shear capacity, $(V_n)_i$, for each yield line i can be obtained as below:

$$(V_n)_i = \frac{bhf_c'}{\left|(X_{ic})_i\right|} \left[\frac{(\nu_e)_i}{2h} F(O')_i + \sum_{j=1}^{N} (\phi_{st})_{ij} (r_s)_{ij} \cos(\alpha_s)_{ij} - \phi_N \left|(Y_{ic})_i\right| \right] \tag{14}$$

where $(\phi_{st})_{ij} = \dfrac{(A_{st})_{ij} (f_y)_{ij}}{bhf_c'}$ = reinforcement index for each individual reinforcing bar j crossing yield line i and $\phi_N \left(= \dfrac{N}{bhf_c'}\right)$ = horizontal load index.

Solution procedure

According to the upper-bound theorem, the collapse occurs at the least strength. The shear capacity of dapped-end beams for different failure planes is implicitly expressed as a function of the position of $(\text{I.C.})_i$, $\left[(X_{ic})_i,(Y_{ic})_i\right]$, as given by Eq. (14). The horizontal $(X_{ic})_i$ and vertical $(Y_{ic})_i$ coordinates of $(\text{I.C.})_i$ for each yield line i are repeatedly tuned until the minimum strength is obtained. The process of adjusting the position of $(\text{I.C.})_i$ for each yield line i is achieved by reliable numerical optimization procedures provided in MATLAB software[14]. The shear capacity of dapped-end beams is the minimum capacity obtained from different mechanisms shown in Fig. 5 and the corresponding yield line is regarded as the critical failure plane.

Fig. 7 shows the variation of normalized shear capacity $V_n / bhf_c^{'}$ of dapped-end beams without shear reinforcement ($A_v = A_h = 0$) and horizontal loads ($N = 0$) against the main longitudinal reinforcement index ϕ_s using the proposed mechanism analysis. For dapped-end beams with a/h of 1.0, the shear capacity can be generally governed by failure plane ① until ϕ_s reaches 0.045, beyond which the shear capacity remains constant as the predicted failure occurs along failure plane ②. On the other hand, the shear capacity of dapped-end beams with a/h of 3.0 is controlled by failure plane ⑤ when ϕ_s is more than 0.015. Mechanism analysis clearly shows that the failure plane and corresponding shear capacity of dapped-end beams are affected by a/h, though the effect of a/h is ignored in PCI design method and is not investigated in tests carried out by several researchers[2-4].

COMPARISONS OF PREDICTED AND MEASURED SHEAR CAPACITIES

Test results of 47 reinforced concrete dapped-end beams were compiled from different experimental investigations carried out by Lu et al.[2], Mattock and Chan[3], Taher[6] and Wang et al.[2]. Table 1 presents the geometrical dimensions, concrete strength and reinforcement details of dapped-end beams considered. Comparisons of measured and predicted shear capacities of dapped-end beams using the three techniques presented above are also given in Table 1 and Fig. 8. The mean $\gamma_{cs,m}$, standard deviation $\gamma_{cs,s}$, and coefficient of variation $\gamma_{cs,v}$ of the ratio between measured and predicted shear capacities of dapped-end beams are presented at the bottom of Table 1. PCI design method and STM model based on ACI 318-05 highly underestimate the shear capacity of dapped end beams. The conservatism of PCI design method increases with the decrease of a_1 / h_d, ϕ_{SH}, and ϕ_s as shown in Fig. 8 as the effect of a_1 / h_d and ϕ_s on the shear capacity of dapped-end beams is not considered in the beam shear failure mode of nib. The shear capacity obtained from STM model based on ACI 318-05 is much lower than experimental results when $\phi_{SH} < 0.2$ as shown in Fig. 8 (b), indicating that shear transfer capacity of hanger reinforcement is underestimated by STM model. On the other hand, predictions obtained from the developed mechanism analysis are less scatter and in better agreement with test results.

PARAMETRIC ANALYSIS

The influence of various parameters on the critical failure plane and corresponding shear capacity of dapped-end beams is investigated using the equations of PCI design method, STM model based on

ACI 318-05, and the developed mechanism analysis. In this parametric study, the width and full depth of beam section, and concrete compressive strength are selected to be fixed at 300 mm, 600 mm, and 30 MPa, respectively. In addition, the shear capacity of dapped-end beams is normalized by $bhf_c^{'}$. It is also to be noted that the shear capacity trend against each parameter predicted below is influenced by the numerical values assigned to other constant parameters of dapped end beams as the failure mode proved to be sensitive to these numerical values.

Effect of dapped end beam geometrical dimensions

The effect of geometrical dimensions on the critical failure plane and corresponding normalized shear capacity $V_n / bhf_c^{'}$ of dapped-end beams without horizontal loads (N =0) is presented in Fig. 9(a) for shear span-to-beam full depth ratio a/h, Fig. 9(b) for effective shear span-to-nib depth ratio a_1 / h_d and Fig. 9(c) for nib depth to beam full depth ratio h_d / h.

Shear span-to-beam full depth ratio a/h**: *Fig. 9(a)***

Predictions obtained from PCI design method remain constant with the variation of a/h for a_1 / h_d = 0.5 and 2.0 as the predicted governing failure occurs in the nib concrete strut (failure plane ② and Eq. 2). For dapped-end beams having a_1 / h_d of 0.5, on the other hand, the normalized shear capacity predicted from the mechanism analysis decreases with the increase of a/h up to a/h of 2.25, which corresponds to the limitation of the inclination of concrete strut (26.5°), beyond which the normalized shear capacity remains constant. However, the shear capacity of dapped-end beams having a_1 / h_d of 2.0 obtained from the mechanism analysis is not affected

by a/h, similar to PCI design method. The effect of a/h on the normalized shear capacity obtained from STM is similar to that observed in the mechanism analysis, though higher shear capacity is predicted by STM. Mechanism analysis and STM clearly show that the shear capacity of dapped-end beams is affected by a/h when failure occurs along diagonal cracks initiated at the bottom corner of the beam full depth as shown in Fig. 5 (e) (failure plane ⑤).

Effective shear span-to-nib depth ratio a_1/h_d **: *Fig. 9(b)***

The normalized shear capacity predicted from PCI design method is not again affected by a_1/h_d when the predicted failure plane is in the concrete strut of nib (failure plane ②) for beams with $A_v = A_h = 0$. On the other hand, the predicted failure is governed by yielding of longitudinal reinforcement of nib (failure plane ①) when both vertical $\phi_v \left(= \frac{A_v f_{yv}}{bhf_c'} \right)$ and horizontal $\phi_h \left(= \frac{A_h f_{yh}}{bhf_c'} \right)$ shear reinforcement indices are 0.03, and a_1/h_d is larger than 1.75, as a result, the shear capacity obtained from the PCI design method decreases with the increase of a_1/h_d. The shear capacity predicted from STM decreases with the increase of a_1/h_d up to a_1/h_d = 2.0, regardless of the amount of shear reinforcement. When $a_1/h_d \geq 2.0$, however, the predictions by STM remains constant as the critical failure plane is formed along the concrete strut of nib (failure plane ②) having the smallest inclination (26.5˚) of concrete strut. On the other hand, shear capacity predictions obtained from the mechanism analysis decrease with the increase of a_1/h_d, regardless of the amount of shear reinforcement, when the failure occurs along the concrete strut of nib as

observed in test results carried out by Lu et al. [2] and Wang et al[7].

Nib depth to beam full depth ratio h_d / h**: Fig. 9(c)**

Predictions obtained from the PCI design method and mechanism analysis increase with the increase of h_d / h when the critical failure plane occurs along the concrete strut of nib, which is also observed in test results carried out by Wang et al[7]. The increasing rate of shear capacity obtained from the mechanism analysis generally increases with the increase of a_1 / h_d, while that of PCI design method is independent on a_1 / h_d. On the other hand, shear capacity predicted from STM decreases with the increase of h_d / h, as the predicted failure is governed by concrete crushing of full depth beam strut (failure plane ⑤).

Effect of dapped end beam reinforcement

Fig. 10 shows the influence of dapped end beam reinforcement on the critical failure plane and corresponding shear capacity of dapped-end beams without horizontal loads (N =0): Fig. 10(a) for longitudinal reinforcement index $\phi_s \left(= \frac{A_s f_{ys}}{b h f_c^{'}} \right) \phi_s$ of nib, Fig. 10(b) for hanger reinforcement index $\phi_{SH} \left(= \frac{A_{SH} f_{ySH}}{b h f_c^{'}} \right)$ and Fig. 10(c) for horizontal shear reinforcement index $\phi_h \left(= \frac{A_h f_{yh}}{b h f_c^{'}} \right)$ of nib.

Longitudinal reinforcement index ϕ_s ***of nib*****: Fig. 10(a)**

The shear capacity predicted from STM and mechanism analysis increases with the increase of ϕ_s up to a certain limit, beyond which it remains constant due to the transition of predicted failure

mode from yielding of longitudinal reinforcement of nib to failure of concrete struts of nib or full depth beam. On the other hand, longitudinal reinforcement of nib has no contribution to the predictions obtained from PCI design method, regardless of a_1 / h_d, when the predicted failure plane is formed along concrete strut of nib.

Hanger reinforcement index ϕ_{SH}**: Fig. 10(b)**

Prediction obtained from PCI design method is not affected by ϕ_{SH}, regardless of a_1 / h_d, as the predicted failure plane is formed along the concrete strut of nib. Shear capacities obtained from STM and mechanism analysis increase with the increase of ϕ_{SH} up to a certain limit (ϕ_{SH} = 0.1 and 0.05 for STM and mechanism analysis, respectively) as failure is governed by yielding of hanger reinforcement. However, failure is predicted to occur in concrete strut of nib with the increase of ϕ_{SH}, as a result, the shear capacities obtained by STM and mechanism analysis are independent on ϕ_{SH}, similar to PCI design method.

Horizontal shear reinforcement index ϕ_h ***of nib***: **Fig. 10(c)**

The shear capacity obtained from PCI design method increases with the increase of ϕ_h, regardless of a_1 / h_d, when failure occurs along the concrete strut of nib. The prediction obtained from STM is independent on ϕ_h, as the shear transfer mechanism of shear reinforcement is not considered. Similarly, prediction obtained from the mechanism analysis is independent on ϕ_h for dapped-end beams having ϕ_h > 0.005 as failure is shifted from concrete strut of nib to concrete strut of full depth for beams.

Effect of Horizontal load

Fig. 11 presents the effect of horizontal tensile load index ϕ_N on the critical failure plane and corresponding normalized shear capacity of dapped-end beams. The shear capacity predicted from PCI design method is not affected by ϕ_N as the predicted failure occurs along the concrete strut of nib. On the other hand, the predictions obtained from mechanism analysis and STM decrease with the increase of ϕ_N. In particular, a far much less decreasing rate of shear capacity is predicted from mechanism analysis with the arrangement of horizontal shear reinforcement of nib. This trend is also confirmed by test results of Mattock and Chan[3].

CONCLUSIONS

A mechanism analysis based on upper-bound theorem is proposed to predict the critical failure plane and corresponding shear capacity of reinforced concrete dapped-end beams. Failure modes observed in experiments are idealized and studied to obtain the shear strength of dapped-end beams. Comparisons between predictions from different techniques and test results of 47 dapped-end beams showed that the shear capacity of dapped-end beams is highly underestimated by PCI design method and the simplified strut-and-tie model based on ACI 318-05, whereas adequately predicted by the proposed mechanism analysis. The mean and standard deviation of the ratio between measured shear capacity and prediction by the mechanism analysis are 0.95 and 0.13, respectively.

PCI design method does not reasonably represent the influence of shear span-to-overall depth ratio of beam, the amount of hanger, longitudinal, and shear reinforcing bars in nib, and horizontal tensile

loads on the shear capacity of dapped-end beams. The trend of shear capacity of dapped-end beams against different parameters predicted by the developed mechanism analysis was similar to that obtained from the strut and tie model. Both the developed mechanism analysis and strut and tie model clearly show that the critical failure plane of dapped-end beams can be altered by different parameters. Furthermore, they point out that the shear capacity of dapped-end beams can be influenced by the shear span-to-overall depth ratio when failure occurs along diagonal cracks originating at the bottom corner of full depth beam, though the shear span-to-overall depth ratio is ignored by PCI design method and is not considered in most test specimens.

ACKNOWLEDGMENTS

This work was supported by the National Research Institute of Cultural Heritage and the Regional Research Centers Program (Bio-housing Research Institute), granted by the Korean Ministry of Education & Human Resources Development.

NOTATION

A_h = area of horizontal shear reinforcement of nib

A_s = area of longitudinal bottom reinforcement

A_{SH} = area of hanger reinforcement

A_v = area of vertical shear reinforcement

a = shear span

a_1 = effective shear span of nib

b = width of beam section

c_b = cover thickness of longitudinal reinforcement in full depth beam

c_t = cover thickness of longitudinal reinforcement in nib

d_d = effective depth of nib

h = overall depth of beam section

h_d = overall depth of nib

$f_c^{'}$ = concrete compressive strength

f_{yh} = yield strength of horizontal shear reinforcement of nib

f_{ys} = yield strength of longitudinal reinforcement of nib

f_{ySH} = yield strength of hanger reinforcement

f_{yv} = yield strength of vertical shear reinforcement of nib

L = length of yield line

l_p = width of loading or support plate

M_n = nominal moment capacity of nib

N = thorizontal tensile force applied at beam support

r = distance between the midpoint of the chord of the yield line and the instantaneous center

r_s = distance between the reinforcing bar crossing a yield line and the instantaneous center

V_n = shear capacity o dapped-end beams

W_c = internal energy dissipated in concrete

W_E = external work done by applied load

W_I = total internal energy dissipated in yield line

W_s = internal energy dissipated in reinforcement

w_{sb} = width of bottom strut of full depth beam

w_{st} = width of nib concrete strut

α = angle between the relative displacement at the midpoints of the chord and yield line

α_s = angle between the relative displacement of the reinforcement about I.C. and the reinforcement crossing a yield line

β = angle between yield line and longitudinal axis

γ = angle between shear reinforcement and the axis of cocrete strut of nib

γ_{cs} = ratio between measured and predicted shear capacities

δ = relative displacement vector across a yield line

δ_s = relative displacement vector of reinforcement crossing a yield line

λ = modification factor to account for the use of lightweight concrete

μ = friction coefficient of concrete

θ = angle between concrete strut and longitudinal axis of beam

ϕ_h = horizontal shear reinforcement index $\left(\frac{A_h f_{yh}}{bhf_c^{'}} \right)$

ϕ_N = horizontal load index $\left(\frac{N}{bhf_c^{'}}\right)$

ϕ_s = longitudinal reinforcement index of nib $\left(\frac{A_s f_{ys}}{bhf_c^{'}}\right)$

ϕ_{SH} = hanger reinforcement index $\left(\frac{A_{SH} f_{ySH}}{bhf_c^{'}}\right)$

ϕ_v = vertical shear reinforcement index $\left(\frac{A_v f_{yv}}{bhf_c^{'}}\right)$

ν_e = effectiveness factor of concrete

ω = relative rotational displacement of rigid block *I* to rigid block *II* about the instantaneous cednter

REFERENCES

1. MacGregor J. G. and Wight J. K. *Reinforced concrete : Mechanics and design*. Prentice-Hall, Pearson Education South Asia Pte Ltd., Singapore, 2005.

2. Lu W. Y., Lin I. J., Hwang S. J. and Lin Y. H. Shear strength of high-strength concrete dapped-end beams. *Journal of the Chinese Institute of Engineers*, 2003, **26**, No. 5, 671-680.

3. Mattock A. H. and Chan T. C. Design and behavior of dapped-end beams. *PCI Journal*,1979, **24**, No. 6, 28-45.

4. Mattock A. H. and Theryo T. S. Strength of precast prestressed concrete members with dapped ends. *PCI Journal*, 1986, **31**, No.5, 58-75.

5. Hamoudi A. A., Phang M. K. S. and Bierweiler R. A. Diagonal shear in prestressed concrete dapped-beams. *ACI Journal*, 1975, **72**, No.7, 347-350.

6. Taher S. E. D. M. F. Strengthening of critically designed girders with dapped ends. *Structures and Buildings*, 2005, **158**, No.2, 141-152.

7. Wang Q., Guo Z. and Hoogenboom P. C. J. Experimental investigation on the shear capacity of RC dapped end beams and design recommendations. *Structural Engineering and Mechanics*, 2005, **21**, No.2, 221-235.

8. PCI Industry Handbook Committee. *PCI design handbook: Precast and prestressed concrete*. Precast/Prestressed Concrete Institute, Chicago (Illinois, USA), 1992.

9. ACI Committee 318. *Building code requirements for structural concrete (ACI 318-05) and commentary (ACI 318R-05).* American Concrete Institute, Farmington Hills, Michigan, USA, 2005.

10. Nielsen M. P. *Limit analysis and concrete plasticity*. Prentice-Hall, Englewood Cliffs, 1984.

11. Ashour A. F. and Morley C. T. The numerical determination of shear failure mechanisms in reinforced concrete beams. *The Structural Engineer*, 1994, **72** No.23&24, 395-400.

12. Bræstrup M. W. Shear strength prediction-plastic method; *Reinforced concrete deep beams*. F. K. Kong, ed.; Blackie and Son Ltd. 1990, 182-203.

13. Yang K. H. and Ashour A. F. Mechanism analysis for shear capacity of reinforced concrete corbels. Submitted to *ACI Structural Journal*, 2007.

14. Chapman S. J. *MATLAB programming for engineers*. Thomson, USA, 2004.

Table 1-Comparison of measured and predicted shear capacities of dapped-end beams.

Researcher	specimen	f_c' (MPa)	b (mm)	h (mm)	h_d (mm)	a_0 (mm)	a/h	a_1/h_d	ϕ_{SH}	ϕ_s	ϕ_v	ϕ_h	ϕ_N	V_n (kN)				$(V_n)_{Exp.}/(V_n)_{pre.}$		
														Exp.	PCI	STM	Mech. anal.	PCI	STM	Mech. anal.
Mattock and Chan	1A	34	127	610	305	114	0.8	0.6	0.074	0.026	0.000	0.011	0.000	144	64	94	147	2.25	1.53	0.98
	1B	31	127	610	305	114	0.8	0.6	0.084	0.099	0.000	0.025	0.056	191	91	141	182	2.10	4.81	1.05
	2A	33	127	610	305	114	0.8	0.6	0.051	0.040	0.000	0.023	0.000	178	94	93	179	1.90	2.31	1.00
	2B	31	127	610	305	114	0.8	0.6	0.056	0.098	0.000	0.025	0.047	169	92	95	166	1.84	11.91	1.02
	3A	37	127	610	305	114	0.8	0.6	0.057	0.035	0.000	0.020	0.000	216	94	116	225	2.30	2.24	0.96
	3B	32	127	610	305	114	0.8	0.6	0.069	0.102	0.000	0.025	0.051	177	95	121	188	1.86	6.27	0.94
	4A	32	127	610	305	114	1.3	0.6	0.068	0.041	0.000	0.023	0.000	189	90	142	177	2.10	1.52	1.07
	4B	29	127	610	305	114	1.3	0.6	0.075	0.109	0.000	0.026	0.055	177	92	174	179	1.92	2.12	0.99
Lu et al.	1	34	200	600	300	80	0.7	0.5	0.134	0.097	0.000	0.026	0.000	561	157	403	540	3.57	1.65	1.04
	2	63	200	600	300	80	0.7	0.5	0.087	0.053	0.000	0.014	0.000	705	176	490	711	4.01	1.80	0.99
	3	69	200	600	300	80	0.7	0.5	0.079	0.048	0.000	0.013	0.000	713	180	490	727	3.96	1.82	0.98
	4	34	200	600	300	160	0.9	0.8	0.087	0.097	0.000	0.026	0.000	360	157	178	380	2.29	2.02	0.95
	5	63	200	600	300	160	0.9	0.8	0.058	0.053	0.000	0.014	0.000	513	176	245	549	2.91	2.22	0.93
	6	69	200	600	300	160	0.9	0.7	0.052	0.048	0.000	0.013	0.000	521	180	255	562	2.89	2.22	0.93
	7	34	200	600	300	80	0.7	0.5	0.108	0.065	0.000	0.026	0.000	458	157	401	529	2.92	1.62	0.87
	8	63	200	600	300	80	0.7	0.5	0.058	0.035	0.000	0.014	0.000	599	176	381	684	3.40	2.16	0.88
	9	69	200	600	300	80	0.7	0.5	0.052	0.032	0.000	0.013	0.000	642	180	381	700	3.57	2.32	0.92
	10	34	200	600	300	160	0.9	0.8	0.073	0.065	0.000	0.026	0.000	291	157	167	320	1.85	1.85	0.91
	11	63	200	600	300	160	0.9	0.8	0.040	0.035	0.000	0.014	0.000	351	176	161	392	1.99	2.28	0.90
	12	69	200	600	300	160	0.9	0.8	0.036	0.032	0.000	0.013	0.000	392	180	161	394	2.18	2.54	0.99

	B1.11	11	214	370	170	75	1.3	0.9	0.182	0.118	0.049	0.000	0.000	59	61	85	63	0.97	0.69	0.93
	B1.12	11	214	370	164	75	1.2	0.8	0.027	0.118	0.049	0.000	0.000	42	24	21	46	1.73	2.61	0.91
	B1.21*	11	220	370	190	75	1.3	1.2	0.316	0.122	0.050	0.000	0.000	65	62	63	79	1.04	1.03	0.83
	B1.22	11	220	370	160	75	1.1	1.0	0.078	0.122	0.050	0.000	0.000	73	60	43	86	1.23	1.88	0.85
	B2.11	13	150	300	150	75	0.8	0.7	0.041	0.180	0.074	0.000	0.000	35	24	13	58	1.42	2.71	0.60
	B2.12	13	150	300	150	75	0.8	1.2	0.041	0.180	0.074	0.000	0.000	32	24	4	44	1.30	5.09	0.72
	B2.21	13	150	300	150	75	0.8	1.0	0.083	0.180	0.074	0.000	0.000	55	49	12	50	1.13	3.44	1.11
	B2.22	13	150	300	150	75	0.8	1.1	0.083	0.180	0.074	0.000	0.000	66	49	8	46	1.35	5.34	1.42
	B2.31*	13	150	300	150	75	0.8	0.9	0.360	0.180	0.074	0.000	0.000	76	55	42	79	1.39	1.44	0.96
	B2.32*	13	150	300	150	75	0.8	1.2	0.360	0.180	0.074	0.000	0.000	65	55	35	65	1.19	1.23	1.01
	B3.11	18	150	315	160	75	1.0	0.8	0.063	0.124	0.051	0.000	0.000	60	54	25	68	1.11	2.30	0.88
Wang and	B3.12	18	150	315	160	75	1.0	0.8	0.078	0.124	0.051	0.000	0.000	70	57	37	73	1.22	2.00	0.95
Guo	B3.21	18	150	300	150	75	1.0	0.9	0.066	0.130	0.053	0.000	0.000	66	54	26	64	1.22	2.47	1.04
	B3.22	18	150	300	150	75	1.0	1.0	0.066	0.130	0.053	0.000	0.000	50	54	18	54	0.93	2.28	0.93
	B3.31	16	150	305	150	75	1.0	0.8	0.133	0.145	0.059	0.000	0.000	52	55	52	63	0.94	1.04	0.83
	B3.32	16	150	305	150	75	1.0	0.9	0.267	0.145	0.059	0.000	0.000	63	55	72	70	1.14	0.87	0.91
	B3.41	16	150	310	100	75	1.0	1.1	0.033	0.142	0.058	0.000	0.000	27	24	15	37	1.10	1.89	0.73
	B3.42	16	150	310	100	75	1.0	1.1	0.033	0.142	0.058	0.000	0.000	26	24	15	35	1.08	1.87	0.75
	B3.51*	16	150	305	155	75	1.0	0.8	0.321	0.145	0.059	0.000	0.000	79	56	76	71	1.40	1.20	1.11
	B3.52*	16	150	305	150	75	1.0	0.8	0.321	0.145	0.059	0.000	0.000	75	55	71	65	1.35	1.13	1.16
	B3.61	15	150	300	150	75	1.0	1.0	0.294	0.155	0.063	0.000	0.000	63	56	74	58	1.13	0.84	1.10
	B3.62	15	150	300	150	75	1.0	0.8	0.149	0.155	0.063	0.000	0.000	93	56	61	91	1.66	1.67	1.03
	B3.71*	15	150	300	150	75	1.0	0.8	0.178	0.155	0.063	0.063	0.000	90	84	69	92	1.07	1.39	0.97
	B3.72*	15	150	300	150	75	1.0	0.8	0.178	0.155	0.063	0.063	0.000	116	92	68	97	1.26	2.00	1.20
Taher	Group Ⅰ-0	24	200	300	150	200	2.2	1.5	0.019	0.03	0.019	0.031	0.000	37.5	21	18	45.7	1.79	2.37	0.95

	Group III-0	25	200	300	150	200	2.2	1.5	0.019	0.03	0.019	0.000	0.000	35	21	18	36.1	1.67	1.82	0.13
	Group IV-0	24	200	300	150	200	2.2	1.5	0.019	0.03	0.000	0.031	0.000	34.5	21	18	41.0	1.64	0.77	0.14
Mean																		1.84	2.37	0.95
Standard deviation																		0.83	1.82	0.13
Coefficient of variation																		0.45	0.77	0.14
Note : * indicates specimens having 45^{o} bent-up shear reinforcement at the interface between nib and full depth of beam.																				

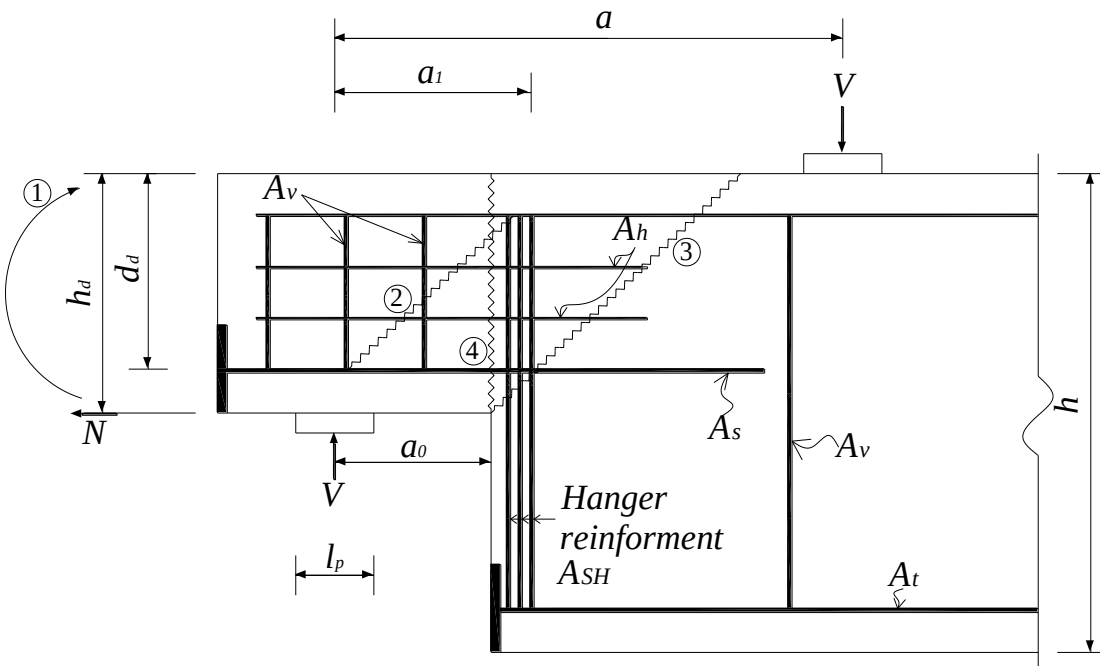

Fig. 1- Potential failure planes of dapped-end beams in PCI design handbook.

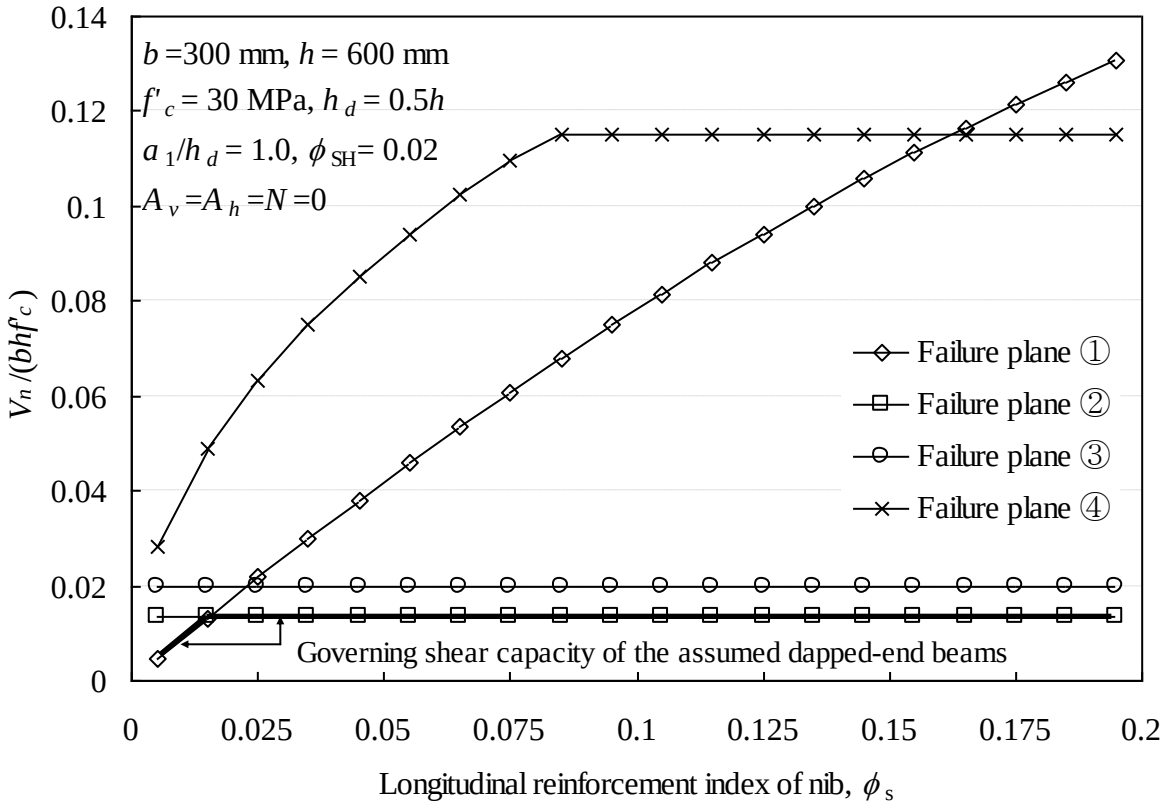

Fig. 2- Effect of ϕ_s on $V_n / bhf_c^{'}$ for different failure planes based on PCI design method.

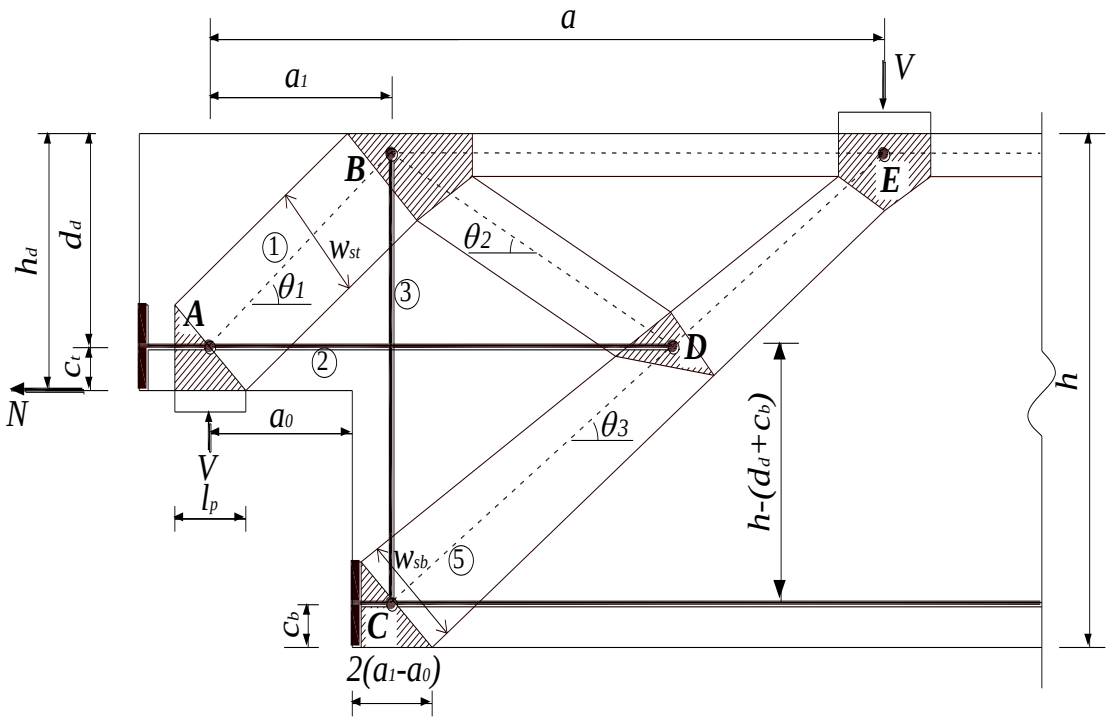

Fig. 3- Schematic strut-and-tie model of dapped-end beams based on ACI 318-05.

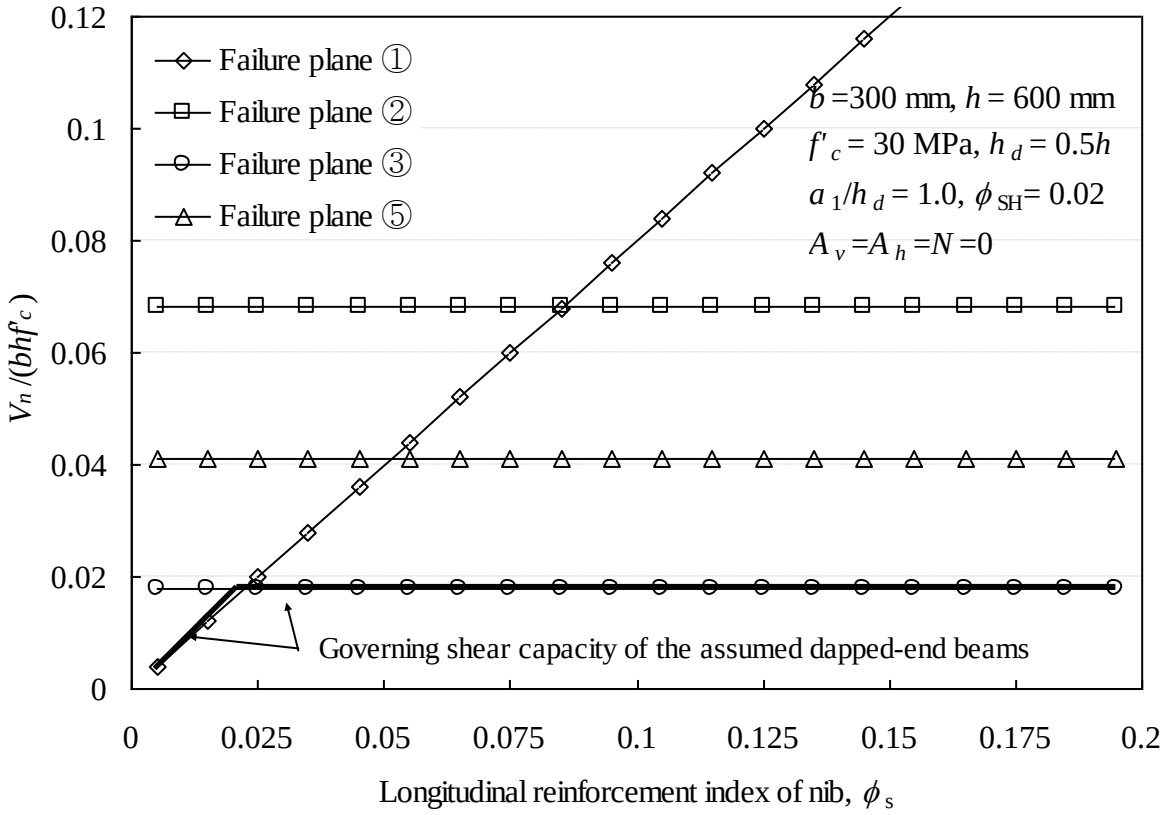

Fig. 4- Effect of ϕ_s on $V_n / bhf_c^{'}$ using strut-and-tie model based on ACI 318-05.

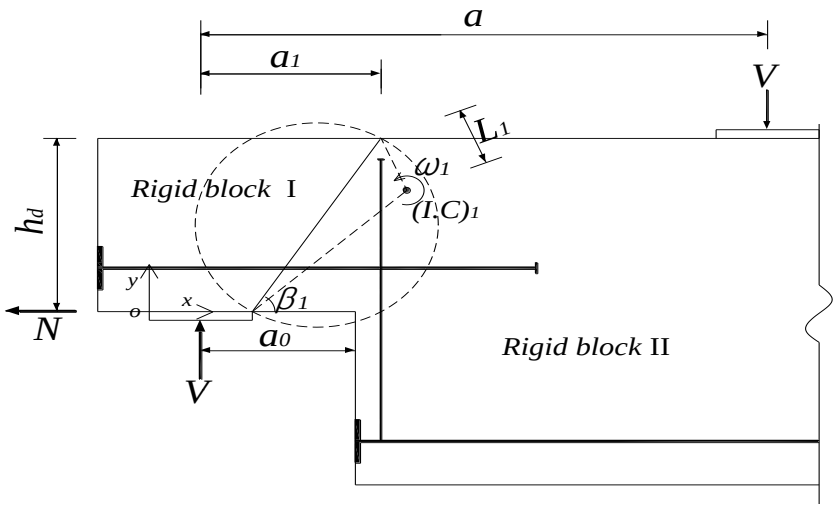

(a) Failure plane ①

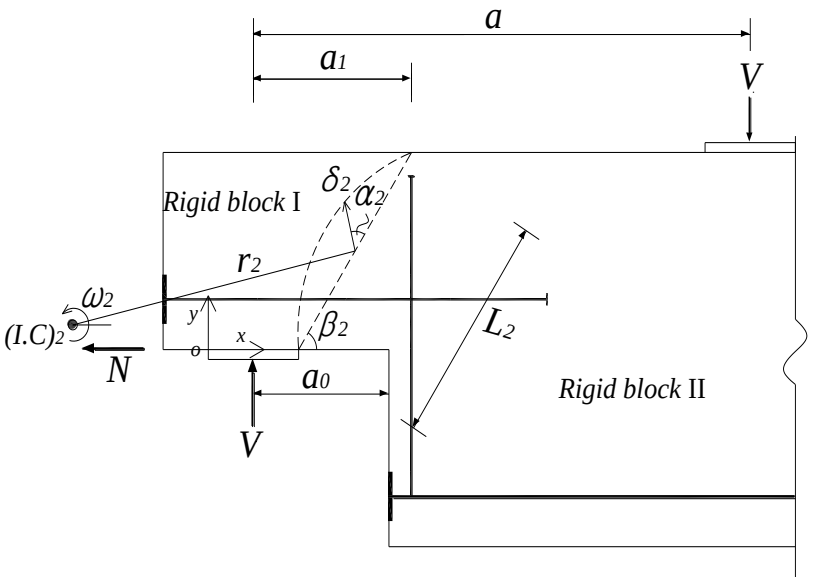

(b) Failure plane ②

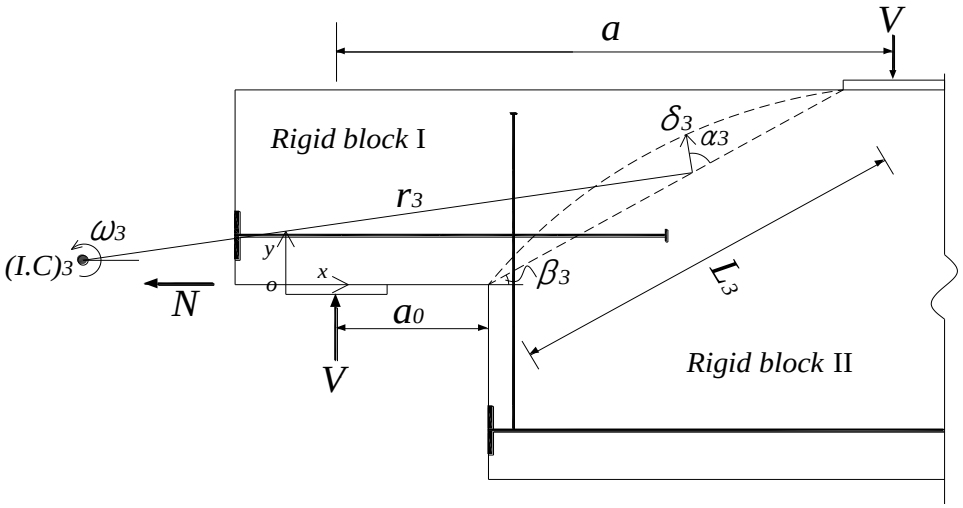

(c) Failure plane ③

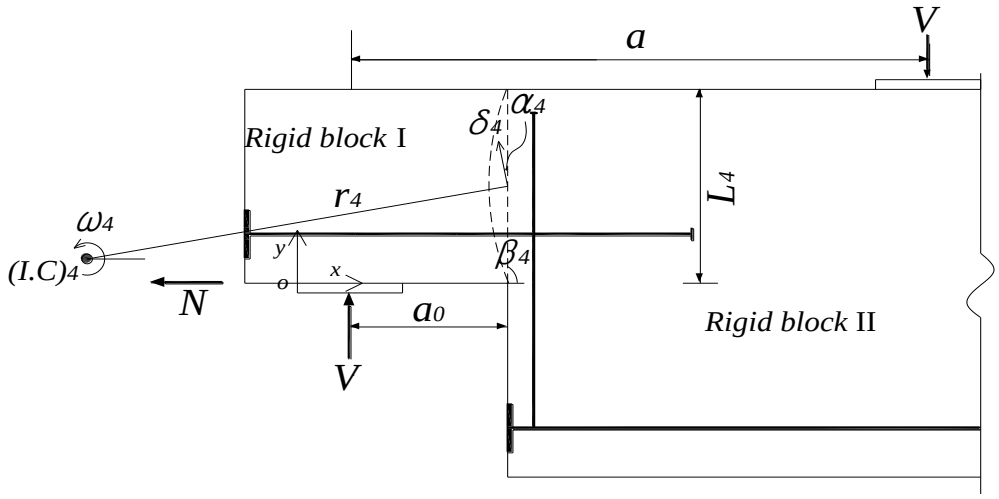

(d) Failure plane ④

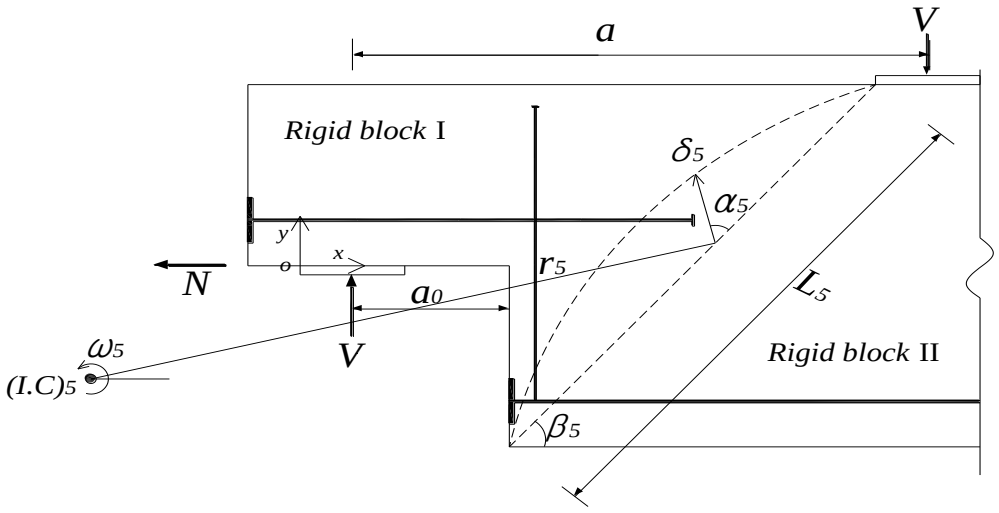

(e) Failure plane ⑤

Fig. 5- Potential failure mechanisms of dapped end beams.

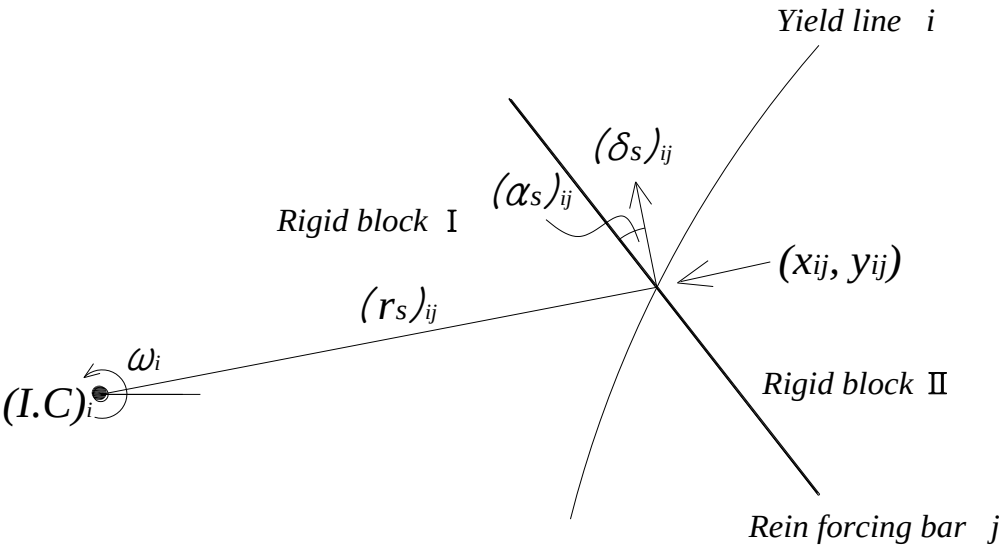

Fig. 6- Reinforcing bar *j* crossing yield line *i*.

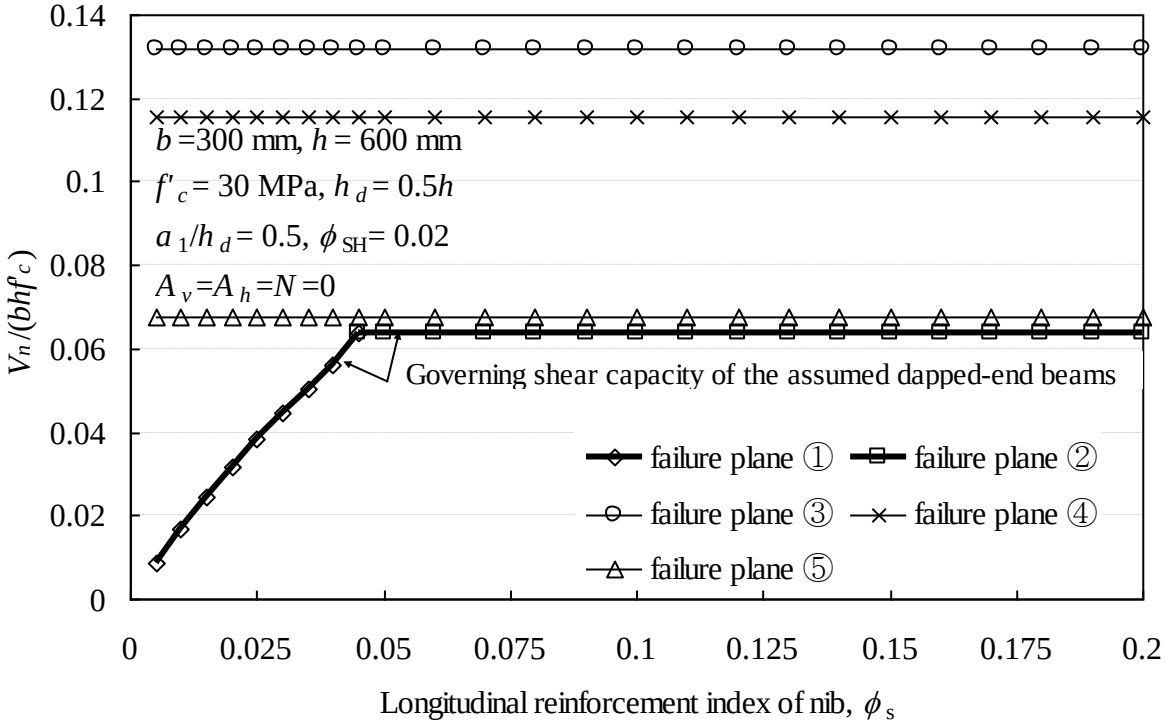

(a) a/h=1.0

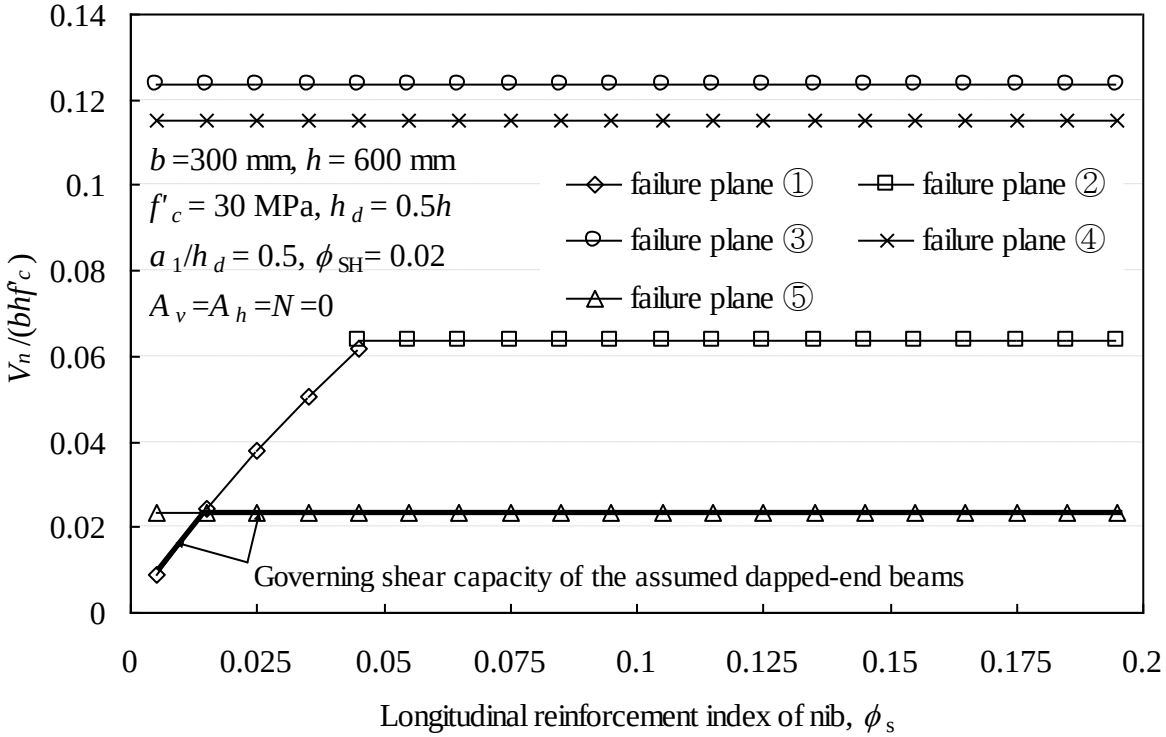

(b) a/h=3.0

Fig. 7- Effect of ϕ_s on $V_n / f_c^{'}bh$ of dapped-end beams using the mechanism analysis.

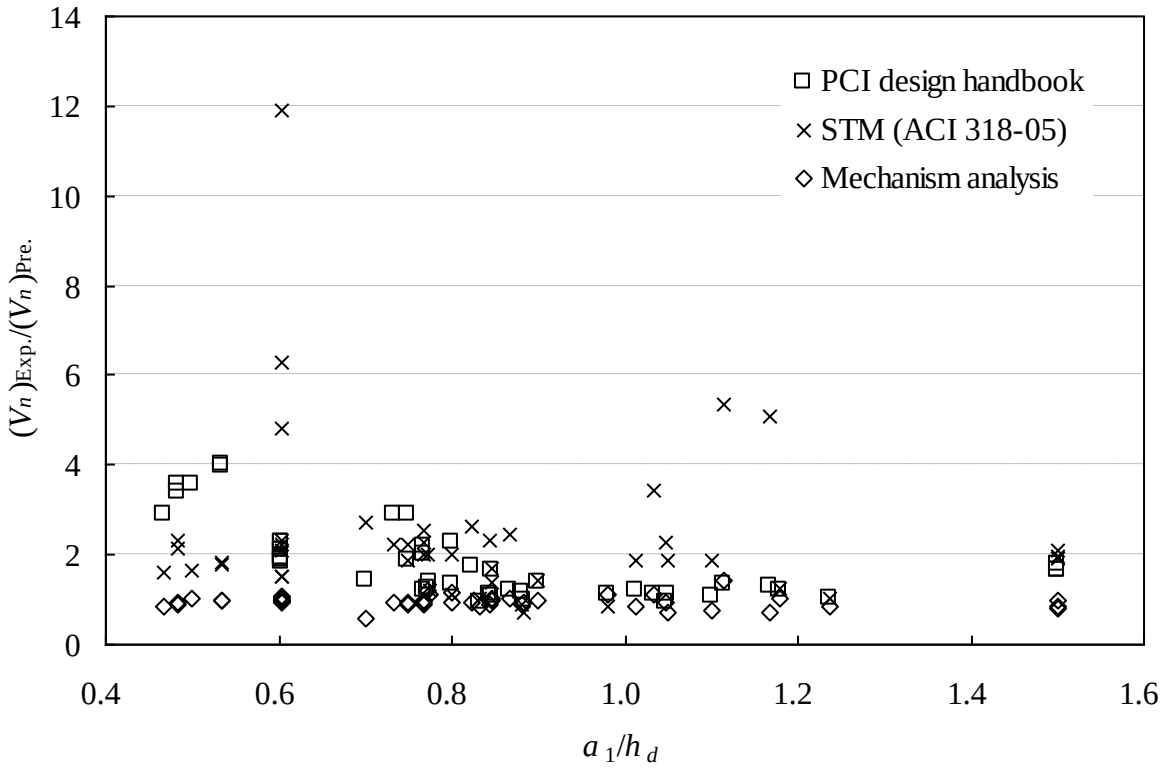

(a) Effect shear span-to-nib depth ratio a_1 / h_d.

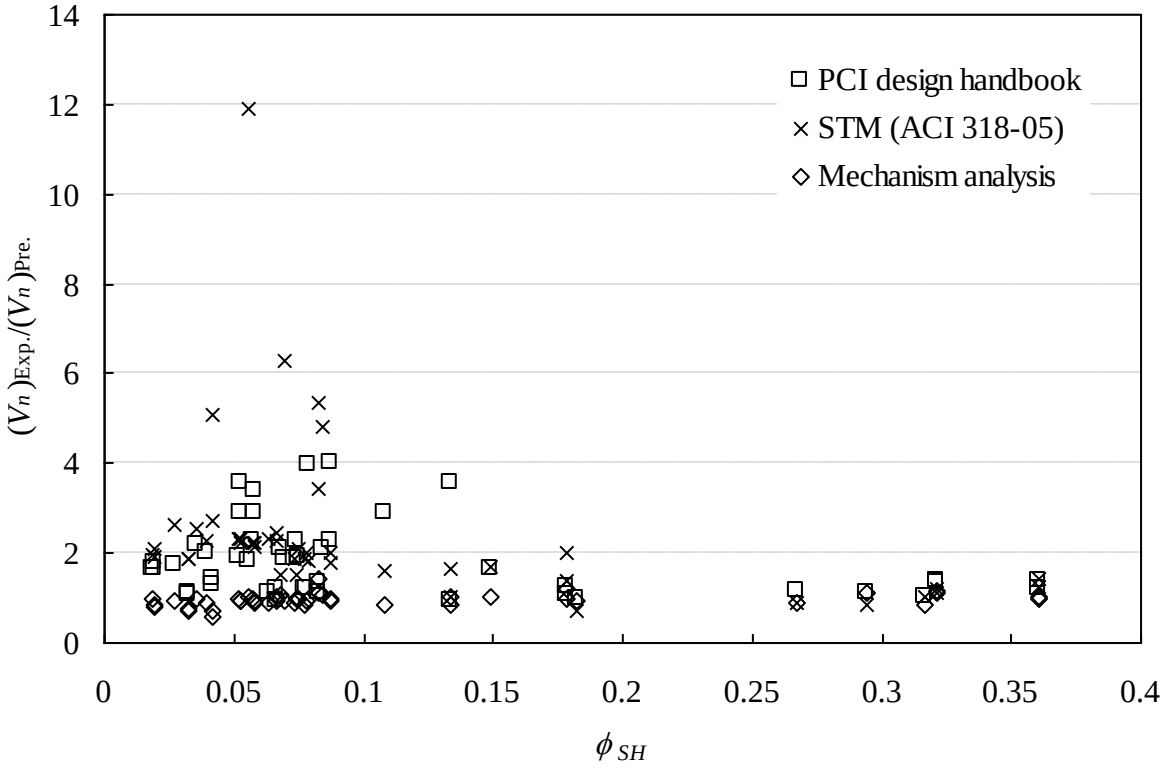

(b) Hanger reinforcement index ϕ_{SH}.

Fig. 8- Comparison of test results with proposed models.

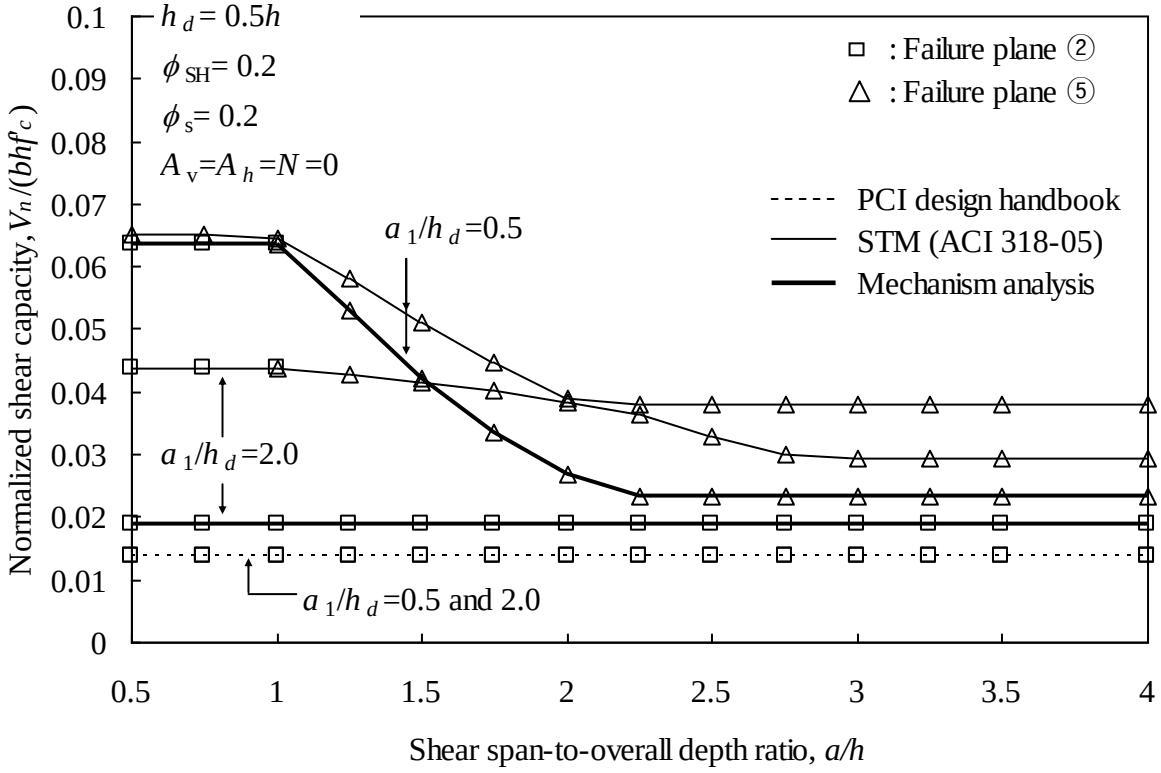

(a) Influence of a/h.

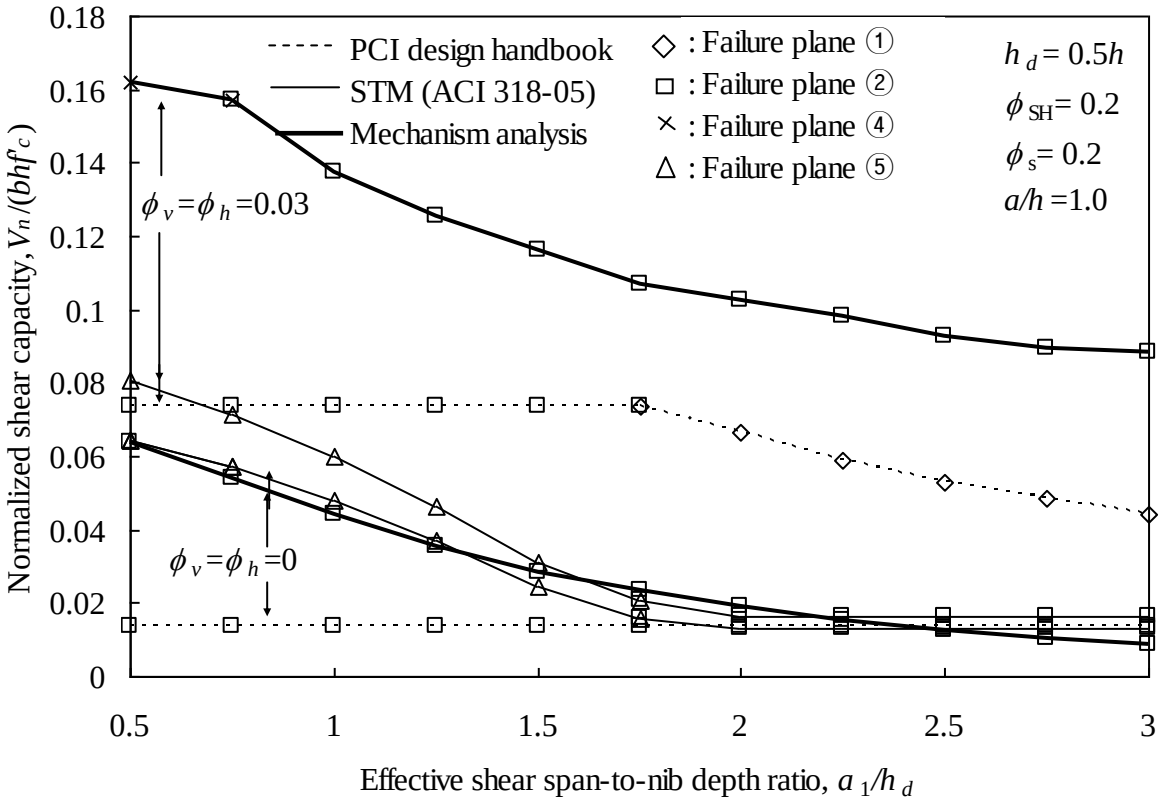

(b) Influence of a_1/h_d.

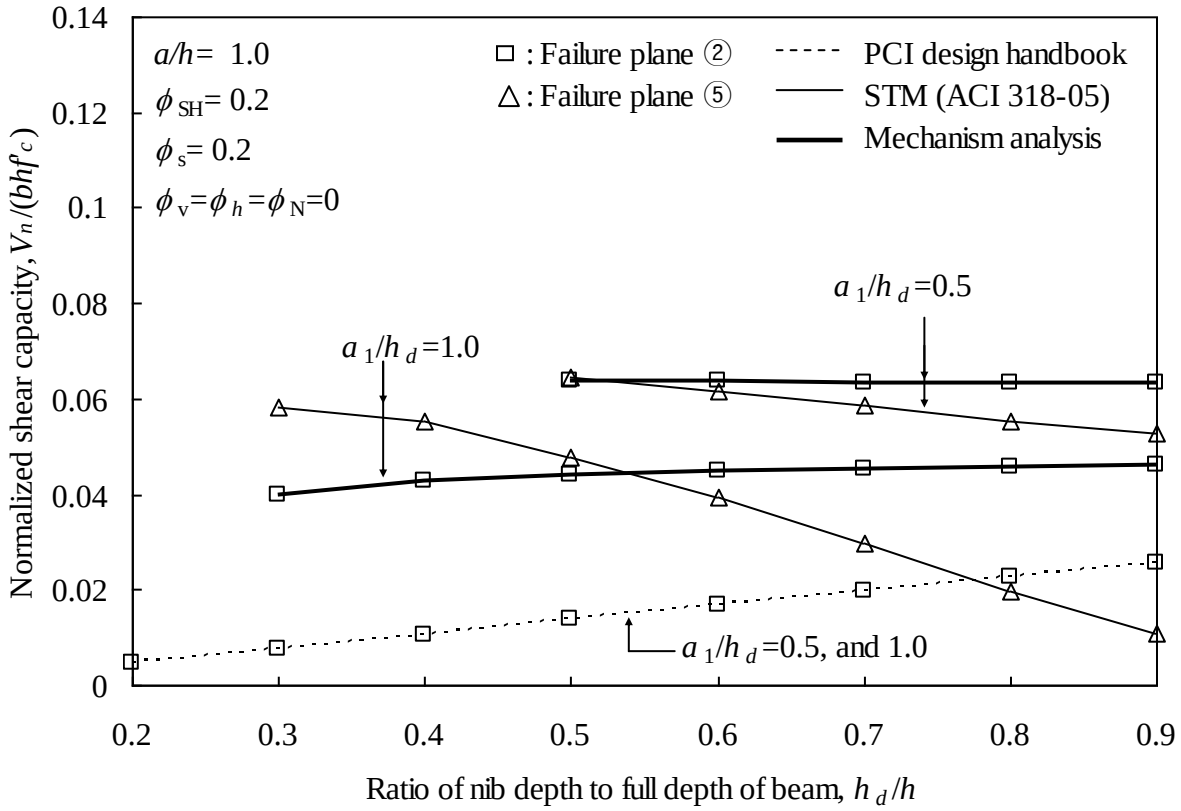

(c) Influence of h_d / h.

Fig. 9- Influence of geometrical dimensions on critical failure plane and shear capacity.

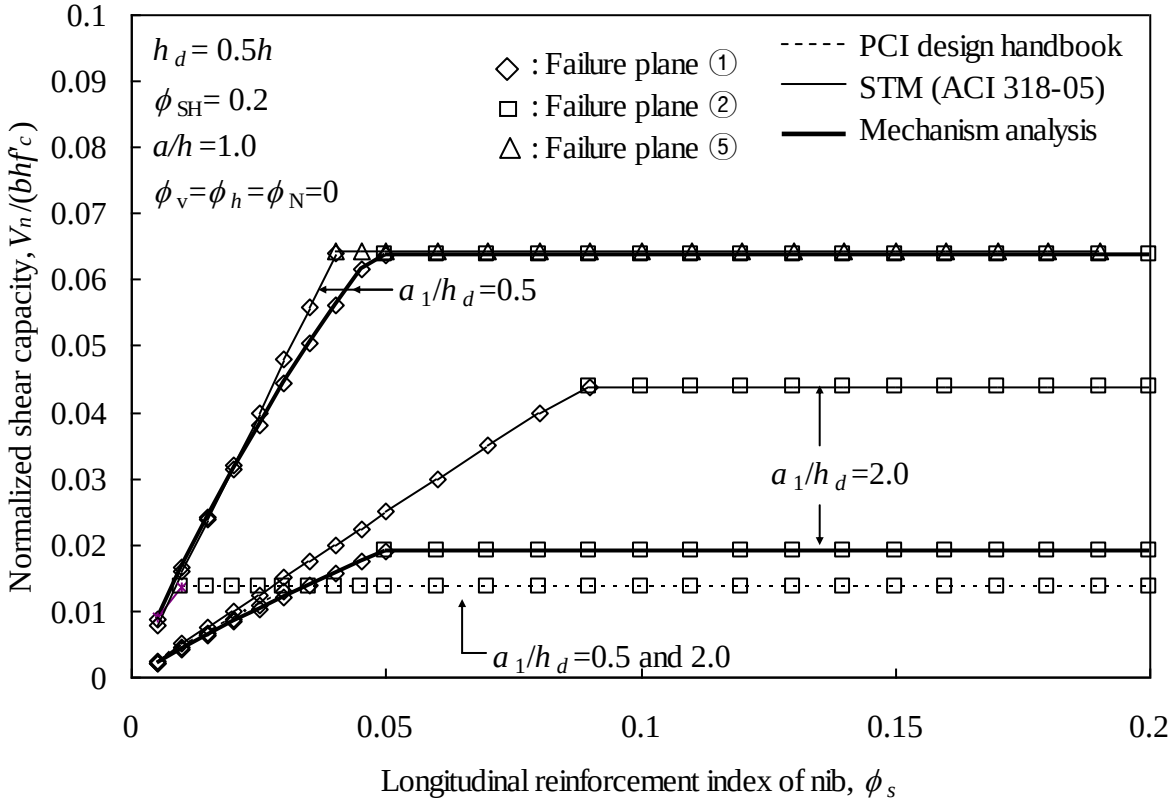

(a) Influence of ϕ_s.

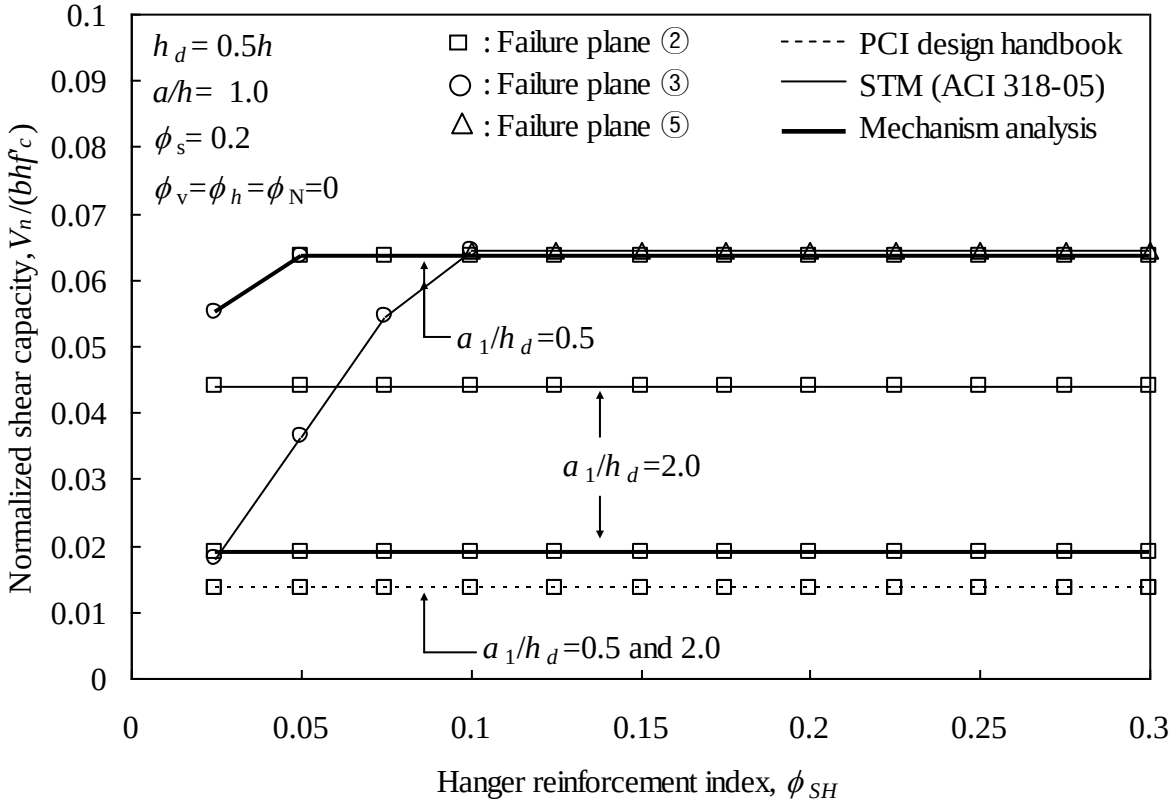

(b) Influence of ϕ_{SH}.

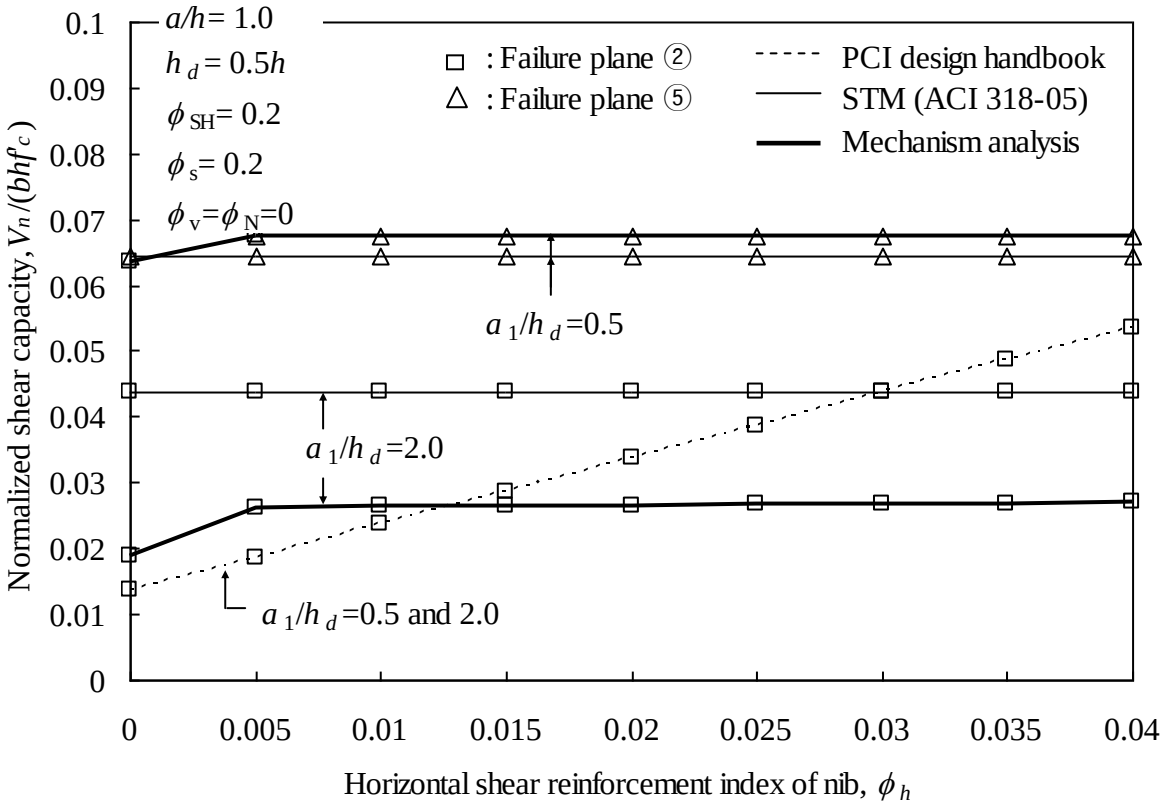

(c) Influence of ϕ_h.

Fig. 10- Influence of dapped end beam reinforcement on critical failure plane and shear capacity.

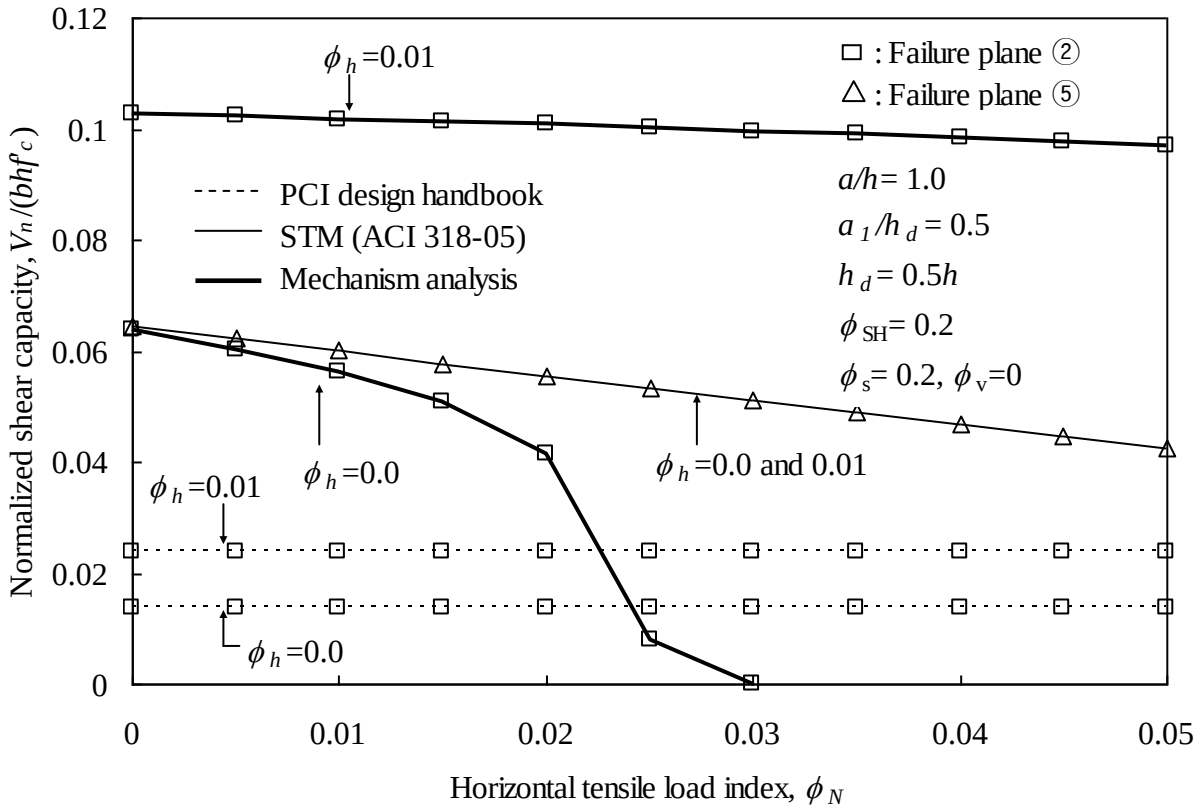

Fig. 11- Influence of ϕ_N on shear capacity.